

## Supporting Information for

### **Coordinative Helix-Helix Association of Heteroleptic Metallosupramolecular Helicates**

*Philjae Kang<sup>b</sup> and Hyojong Yoo<sup>\*a</sup>*

[a] Department of Materials Science and Chemical Engineering, Hanyang University, Ansan-si, Gyeonggi-do, 15588, Republic of Korea.

[b] Department of Chemistry, Yonsei University, Seoul, 03722, Republic of Korea.

\*Correspondence to: [hjhaha73@hanyang.ac.kr](mailto:hjhaha73@hanyang.ac.kr)

### Single crystal X-ray diffraction analysis of $[\text{Ni}_8(\text{PDA})_6(\text{CDBA})_3(\text{DMF})_2(\text{H}_2\text{O})_4]$ (**1**)

Diffraction data from the dark purple crystals of **1** ( $0.279 \times 0.208 \times 0.2 \text{ mm}^3$ ) mounted on a MiTeGen MicroMount© are collected at 100 K on a ADSC Quantum 210 CCD diffractometer equipped with a synchrotron radiation source ( $0.70000 \text{ \AA}$ ) at the Supramolecular Crystallography beamline 2D, Pohang Accelerator Laboratory (PAL), Pohang, Korea. The ADSC Q210 ADX program<sup>1</sup> is used for data collection (detector distance is 63 mm, omega scan;  $\Delta\omega = 1^\circ$ , exposure time is 1 sec/frame for **1**, and HKL3000sm (Ver. 703r)<sup>2</sup> is used for cell refinement, reduction, and absorption correction. The crystal structure of **1** is solved using the direct method with SHELX-XT (Ver. 2014/5)<sup>3</sup> and refined using full-matrix least-squares calculations with the SHELX-XL (Ver. 2014/7)<sup>4</sup> program package.

The systematic absences in the diffraction data are uniquely consistent with orthorhombic, space group Pbcn, yielding chemically reasonable and computationally stable refinement results.<sup>4,5</sup>

The successful solution of the structure by direct methods provides most of the non-hydrogen atoms from the *E*-map. The remaining non-hydrogen atoms are located through an alternating series of least-squares cycles and difference Fourier maps. All the non-hydrogen atoms are refined with anisotropic displacement coefficients. All the hydrogen atoms are included in the structure factor calculation at idealized positions, and allowed to ride on the neighboring atoms with relative isotropic displacement coefficients. The voids contain disordered DMF with a partial occupancy. A satisfactory disorder model for the solvent is not observed; therefore, the solvent mask function in Olex2 is used to mask the disordered density. The final least-squares refinement of 705 parameters against 29843 data results in residuals *R* (based on  $F^2$  for  $I \geq 2\sigma$ ) and *wR* (based on  $F^2$  for all of the data) of 0.0619 and 0.1854 respectively. The final difference Fourier map was featureless.

### Single crystal X-ray diffraction analysis of $\{[\text{Ni}_8(\text{PDA})_6(\text{CDBA})_3(\text{DMF})_4]_2[\text{Ni}(\text{PDA})_2]_2\}$ (**2**)

Diffraction data from the dark purple crystals of **2** ( $0.048 \times 0.059 \times 0.051 \text{ mm}^3$ ) mounted on a MiTeGen MicroMount© are collected at 100 K on a ADSC Quantum 210 CCD diffractometer equipped with a synchrotron radiation source ( $0.70000 \text{ \AA}$ ) at the Supramolecular Crystallography beamline 2D, Pohang Accelerator Laboratory (PAL), Pohang, Korea. The ADSC Q210 ADX program<sup>1</sup> is used for data collection (detector distance is 63 mm, omega scan;  $\Delta\omega = 1^\circ$ , exposure time is 1 sec/frame for **2**, and HKL3000sm (Ver. 703r)<sup>2</sup> is used for cell refinement, reduction, and absorption correction. The crystal structure of **2** is solved using the direct method with SHELX-XT (Ver. 2014/5)<sup>3</sup> and refined using full-matrix least-squares calculations with the SHELX-XL (Ver. 2014/7)<sup>4</sup> program package.

The systematic absences in the diffraction data are uniquely consistent with monoclinic, space group  $P2_1/n$ , yielding chemically reasonable and computationally stable refinement results.<sup>4,5</sup>

The successful solution of the structure by direct methods provides most of the non-hydrogen atoms from the  $E$ -map. The remaining non-hydrogen atoms are located through an alternating series of least-squares cycles and difference Fourier maps. All the non-hydrogen atoms are refined with anisotropic displacement coefficients. All the hydrogen atoms are included in the structure factor calculation at idealized positions, and allowed to ride on the neighboring atoms with relative isotropic displacement coefficients. The voids contain disordered DMF with a partial occupancy. A satisfactory disorder model for the solvent is not observed; therefore, the solvent mask function in Olex2 is used to mask the disordered density. The final least-squares refinement of 1854 parameters against 57564 data results in residuals  $R$  (based on  $F^2$  for  $I \geq 2\sigma$ ) and  $wR$  (based on  $F^2$  for all of the data) of 0.0789 and 0.2440 respectively. The final difference Fourier map was featureless.

## Elemental Analysis

### Compound 1;

Anal. Calcd. for  $C_{114}H_{107}N_{15}Ni_8O_{49}$  ( $[Ni_8(PDA)_6(CDBA)_3(DMF)_5(H_2O)_1]$ , 4DMF): C, 46.56; H, 3.67; N, 7.14, Found: 46.82; H, 3.95; N, 6.94.

### Compound 2;

Anal. Calcd. for  $C_{227}H_{185}N_{25}Ni_{18}O_{113}$   
( $[ \{ Ni_8(PDA)_6(CDBA)_3(DMF)_3(H_2O)_1 \}_2 \{ Ni(PDA)_2 \}_2 (DMA)_2$ , DMF, 10H<sub>2</sub>O): C, 44.50; H, 3.04; N, 5.71, Found: 44.73; H, 4.13; N, 5.41.

**Table S1.** The calculated values through the bond valence sum analysis for metal ions in **1** and **2**

<b>Compounds</b>	<b>Bond valence sum</b>	
<b>1</b>	Ni1	2.01
	Ni2	2.02
	Ni3	2.03
	Ni4	1.96
<b>2</b>	Ni1	1.98
	Ni2	1.97
	Ni3	1.96
	Ni4	1.99
	Ni5	1.97
	Ni6	1.97
	Ni7	2.00
	Ni8	1.99
	Ni9	2.23

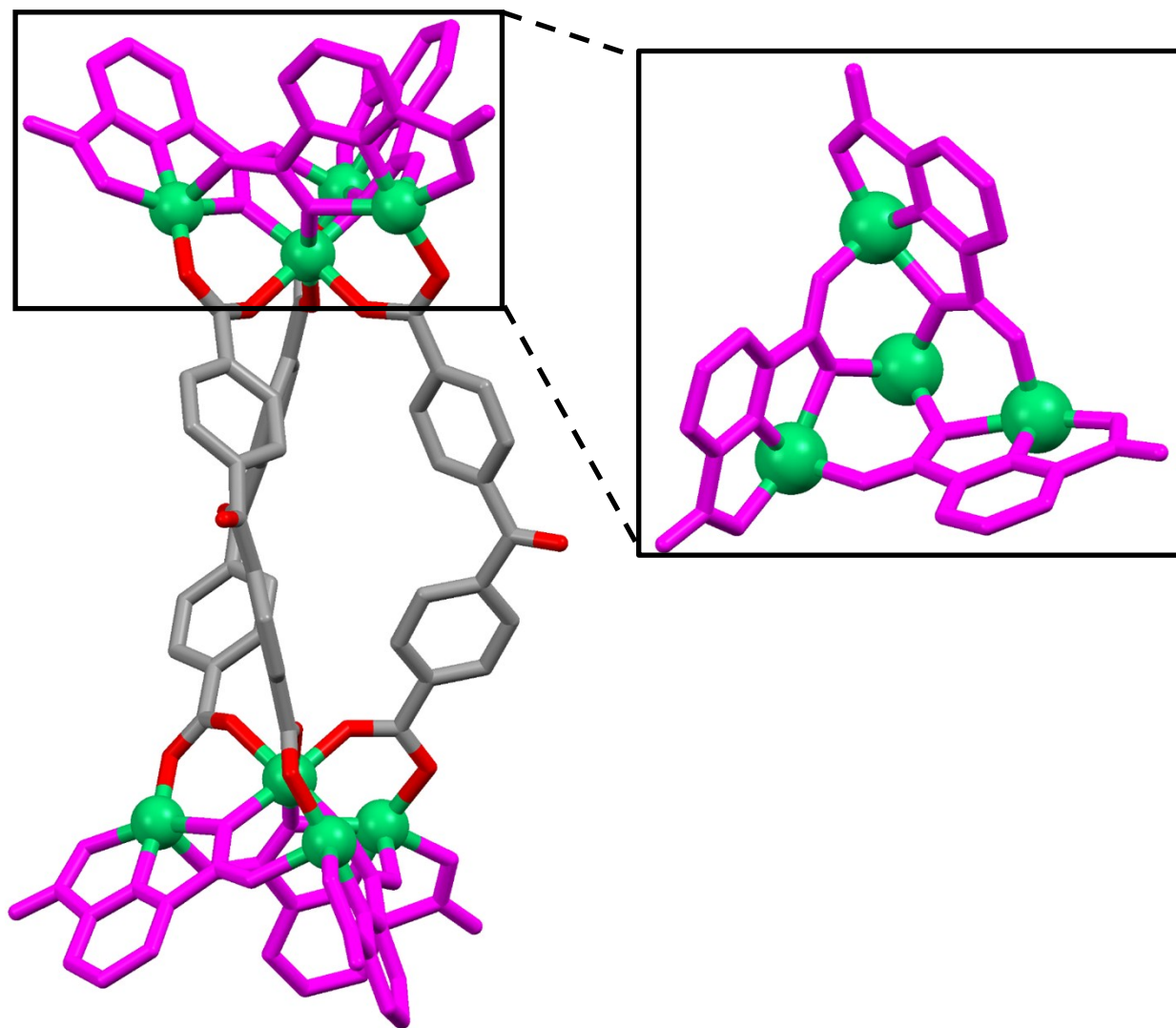
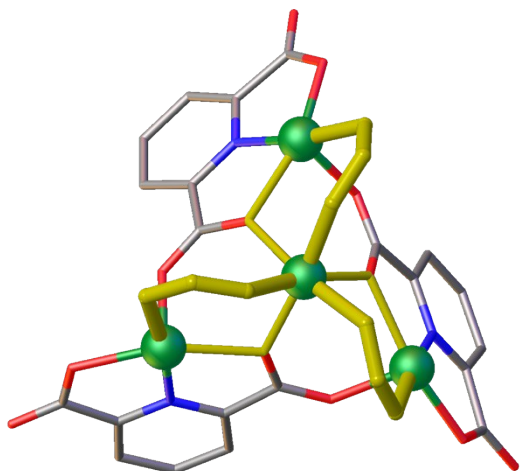
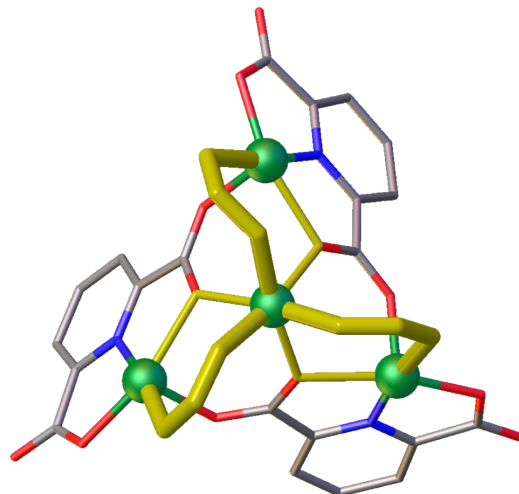


**Fig. S1.** The helical configuration (left-handed) of **1**. The two tetranuclear  $\{\text{Ni}_4\}$  clusters (colored in pink for clarity) are interconnected by three **CDBAs**. Inset reveals a  $\{\text{Ni}_4\}$  cluster from a top-down view, which is assembled from four nickel atoms and three PDAs. The green spheres illustrate the nickel atoms.



$\Lambda$  Isomer



$\Delta$  Isomer

**Fig. S2.** Two chiral conformations of the central Ni atom in  $\{\text{Ni}_4\}$  clusters. The central Ni atom in  $\{\text{Ni}_4\}$  cluster shows both characters of counterclockwise ( $\Lambda$ ) and clockwise ( $\Delta$ ) in **1**.

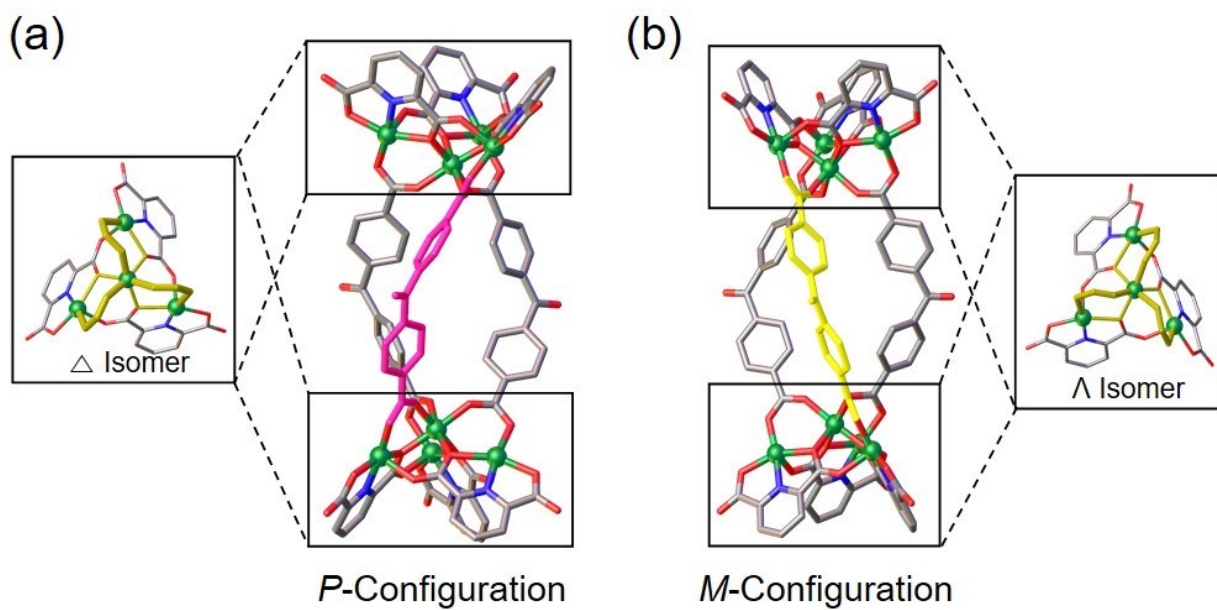


**Fig. S3.** (a) The interconnection of two identical  $\Delta$  isomers by three CDBAs results in the formation of *M*-helicate ( $\Lambda\Lambda$  conformation) and (b) the interconnection of two  $\Delta$  isomers lead to the formation of *P*-helicate ( $\Delta\Delta$  conformation).

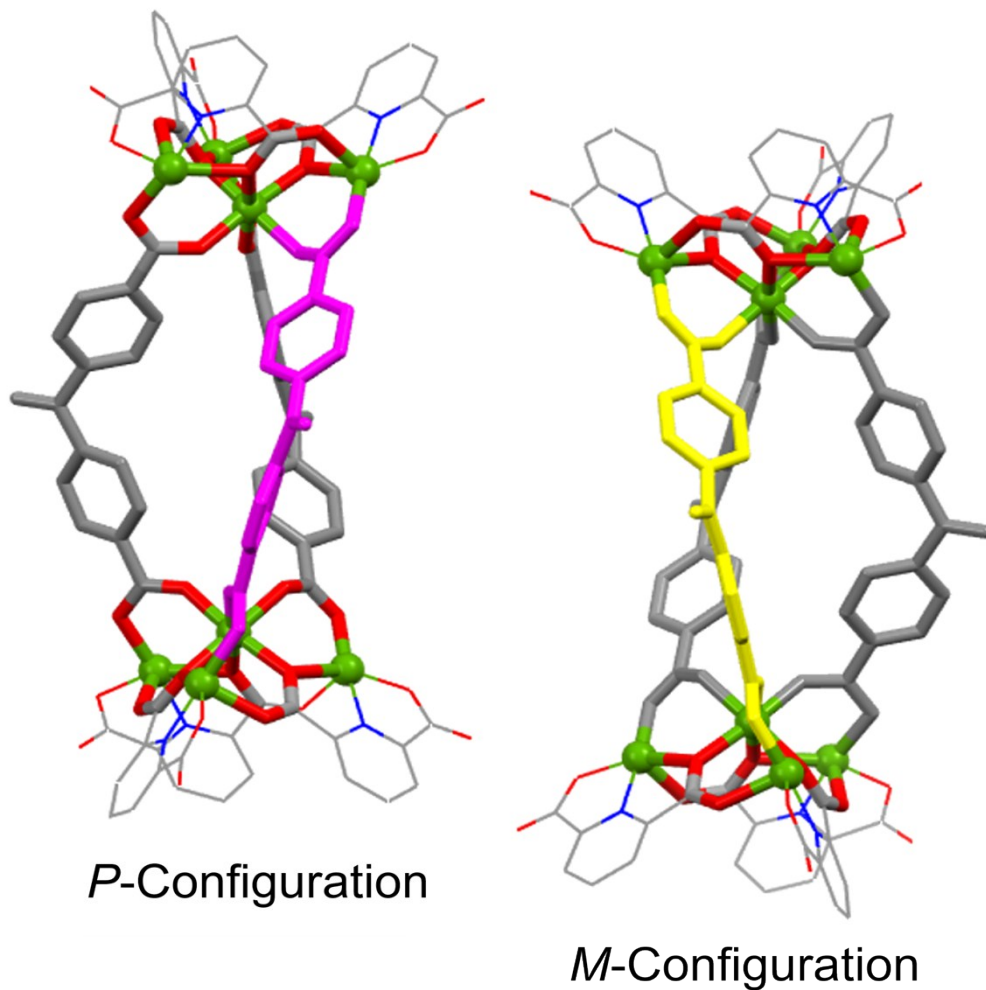


**Fig. S4.** *P*- and *M*- configurations in **1**. The two tetranuclear  $\{\text{Ni}_4\}$  clusters are interconnected by three CDBAs. Both the *P*-helical conformation with  $\Lambda\Lambda$  configuration and *M*-helical conformation with  $\Delta\Delta$  configuration are simultaneously observed in a unit cell. The green spheres illustrate the nickel atoms. One of the CDBAs in each conformation is colored in pink and yellow respectively for clearly distinguishing the orientation (left- and right-handed) of CDBAs in the structure.

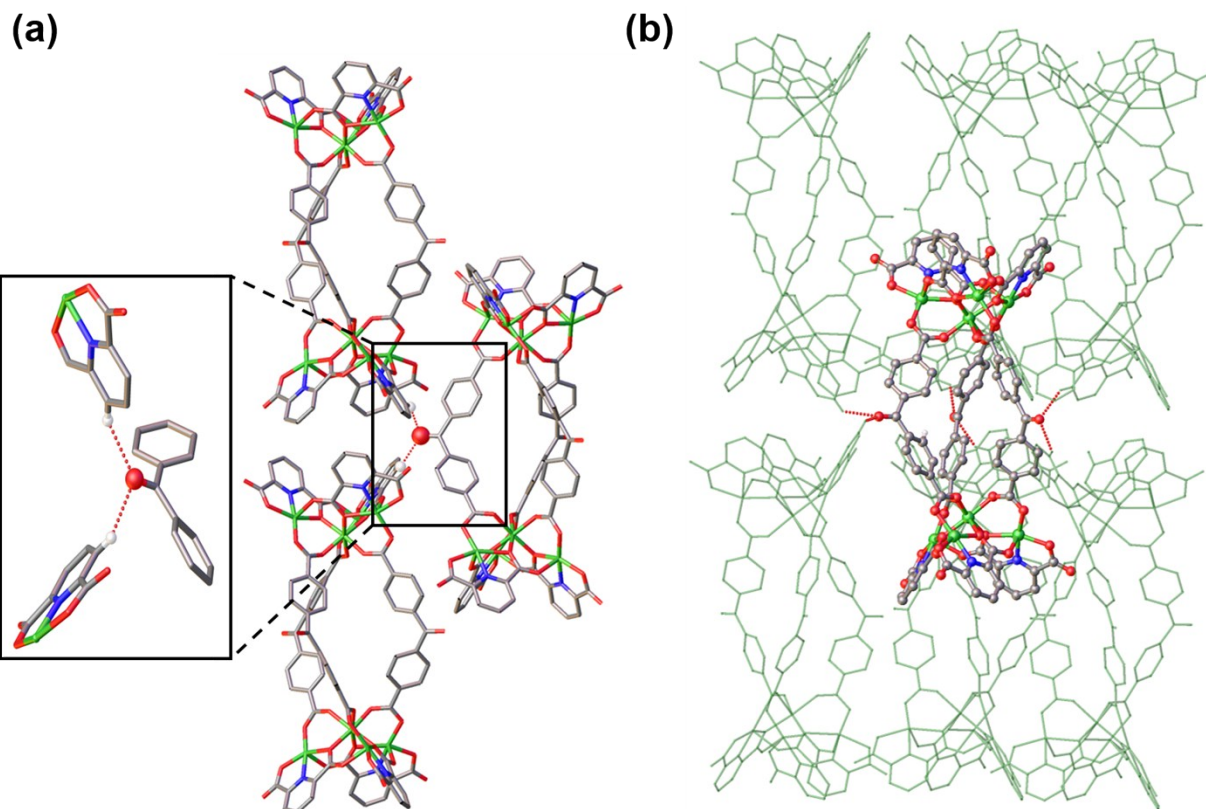


**Fig. S5.** Illustrations of intermolecular hydrogen bonds between between the aromatic hydrogen atom in PDA and oxygen atom of C=O in CDDBA. One oxygen atom in CDDBA linker interacted with two supramolecular helicates (a). One helicate connects neighboring six helicates (b).

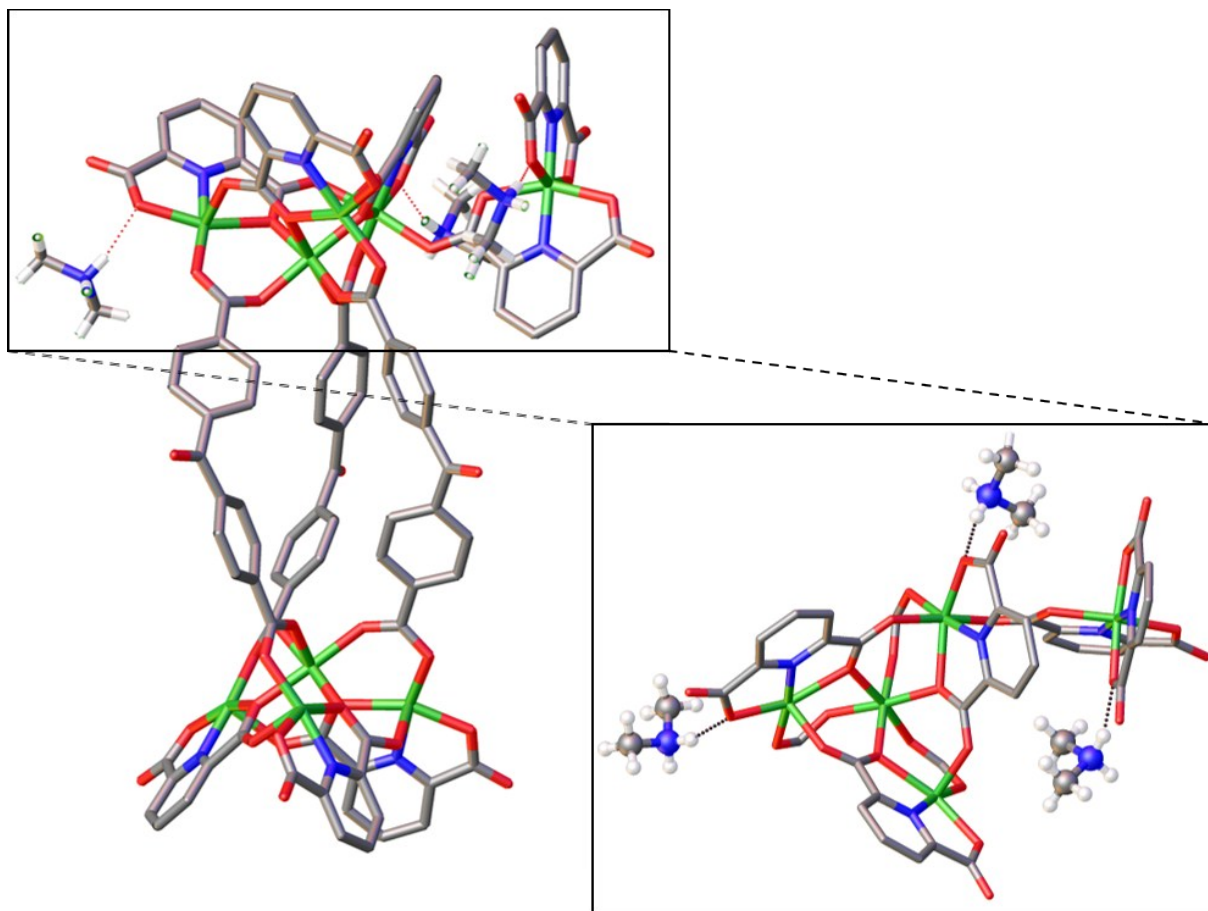


**Fig. S6.** Asymmetric unit of **2**. There are half of molecule **2** and three crystallographically different dimethylammonium cations ( $(\text{CH}_3)_2\text{NH}_2^+$ ,  $\text{DMA}^+$ ) are presented. Inset represents the hydrogen bonding between three  $\text{DMA}^+$  and **2** from top-down view, where a  $\text{DMA}^+$  ion interacts with an oxygen atom in  $[\text{Ni}(\text{PDA})_2]$  linker and two  $\text{DMA}^+$  interact with two oxygen atoms in the two PDAs bonded to the independent  $\{\text{Ni}_4\}$  cluster.

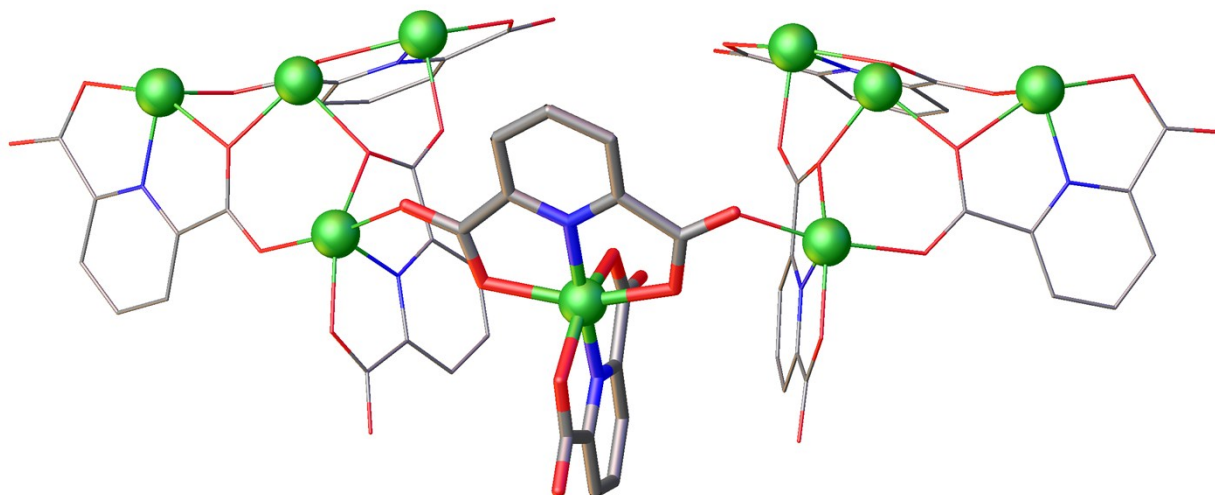


**Fig. S7.** Bridging mode of metalloligand  $[\text{Ni}(\text{PDA})_2]$  in molecular structure of **2**. Two  $\{\text{Ni}_4\}$  clusters are connected by bridging ligand  $[\text{Ni}(\text{PDA})_2]$ , where two oxygen atoms of a PDA in  $[\text{Ni}(\text{PDA})_2]$  are coordinated to Ni atoms from two different  $\{\text{Ni}_4\}$  clusters.

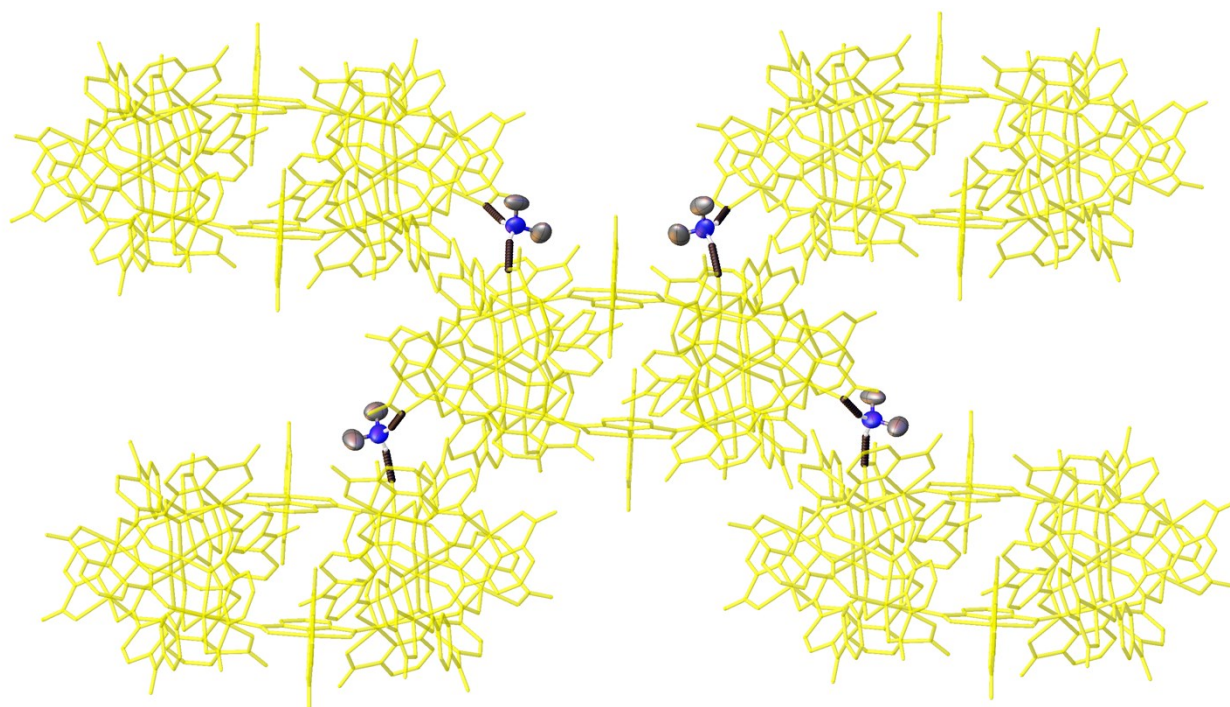


**Fig. S8.** Illustrations of intermolecular hydrogen bonds in the packing structure of **2**. The macrocycle **2** acts as hydrogen acceptor and DMA<sup>+</sup> ion (hydrogen donor) connects two adjacent macrocycles by NH $\cdots$ O hydrogen bonding.

A single DMA<sup>+</sup> strongly interacts with an oxygen atom in a [Ni(PDA)<sub>2</sub>] linker by NH $\cdots$ O bonding with a N(177)  $\cdots$ O(11) distance of 2.77 Å. Other DMA<sup>+</sup>s interact with two oxygen atoms in the two PDAs, which are bonded to an independent {Ni<sub>4</sub>} cluster by NH $\cdots$ O hydrogen bonding with an average distance of 2.8 Å.

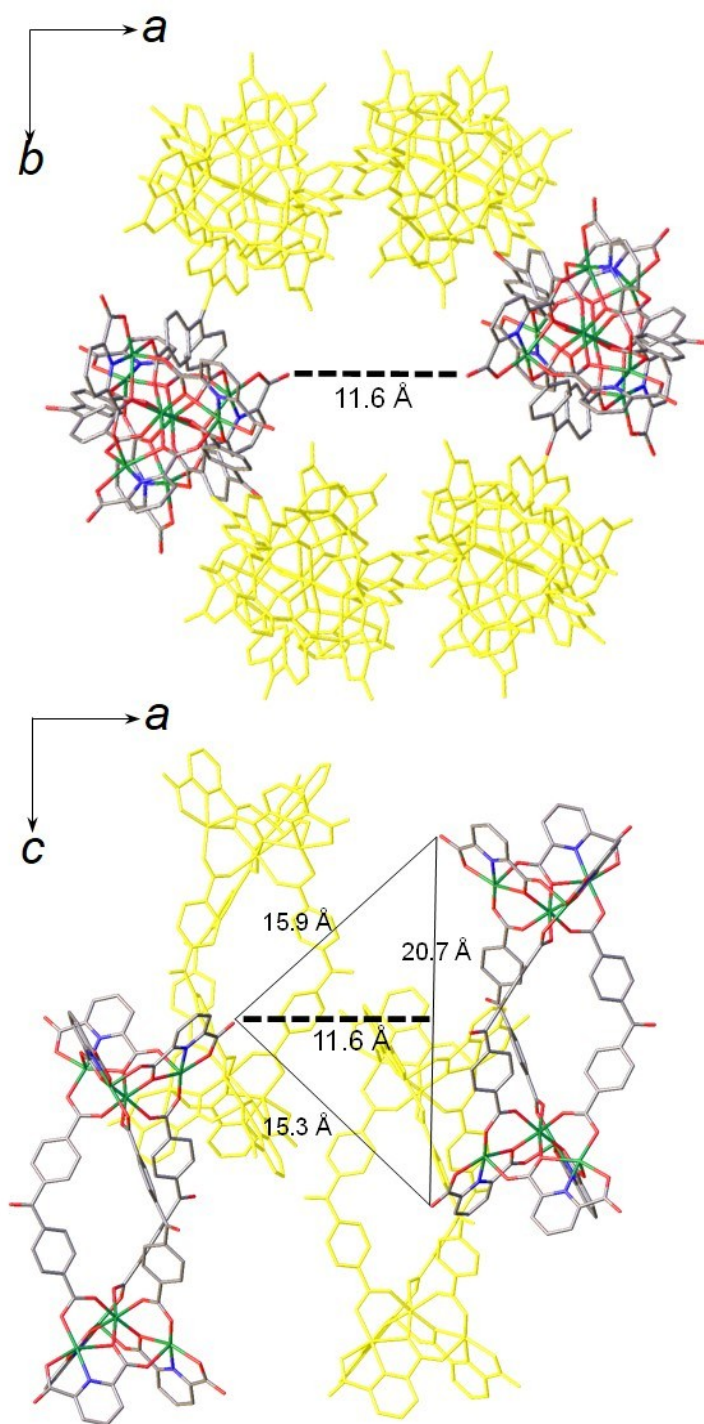


**Fig. S9.** Packing structure of **1** and the channel dimension measurement in **1**. The pore dimension estimated is 11.6 Å

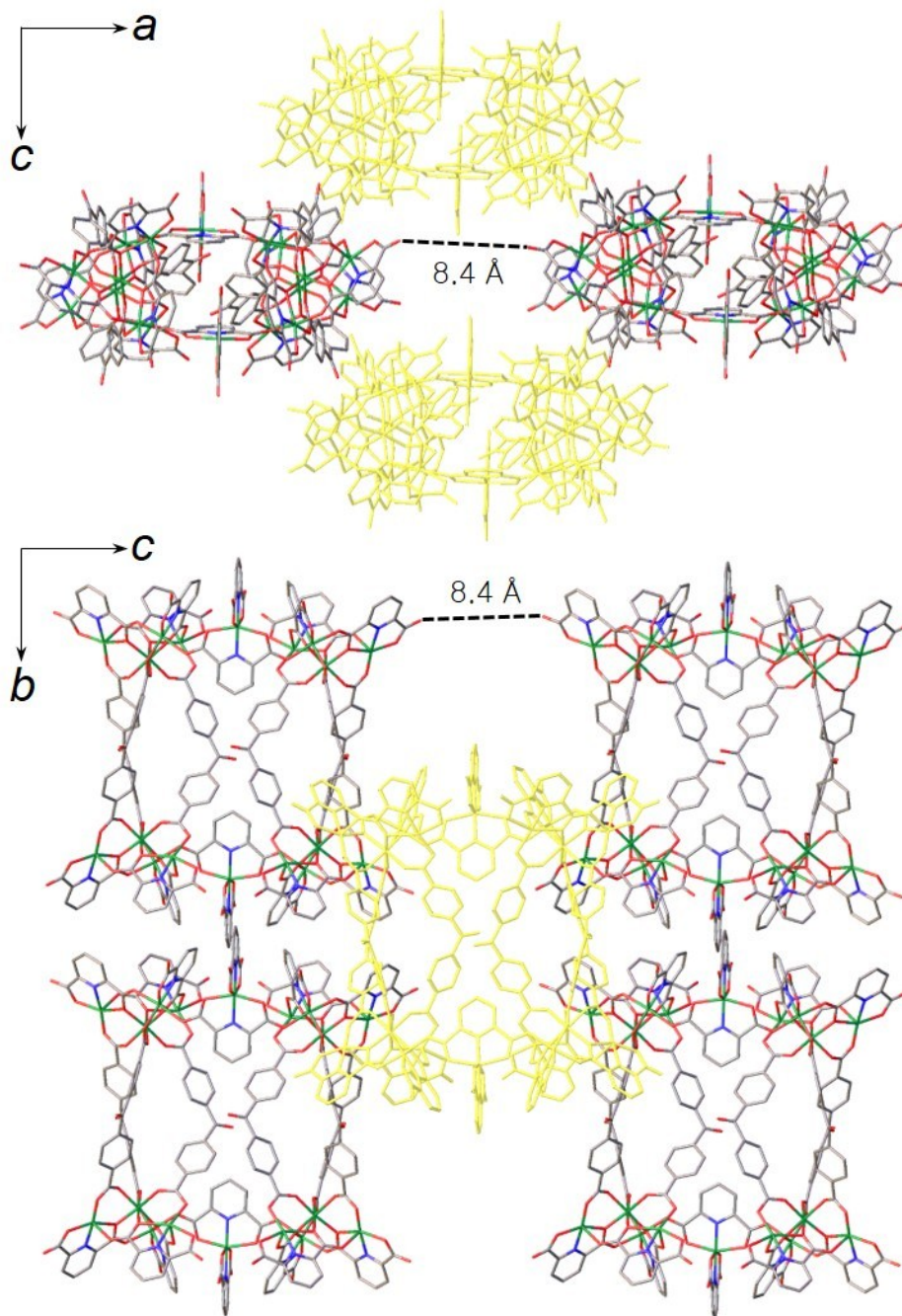


**Fig. S10.** Packing structure of **1** and the channel dimension measurement in **1**. The pore dimension estimated is 8.4 Å from intermolecular O $\cdots$ O distance across the pore.

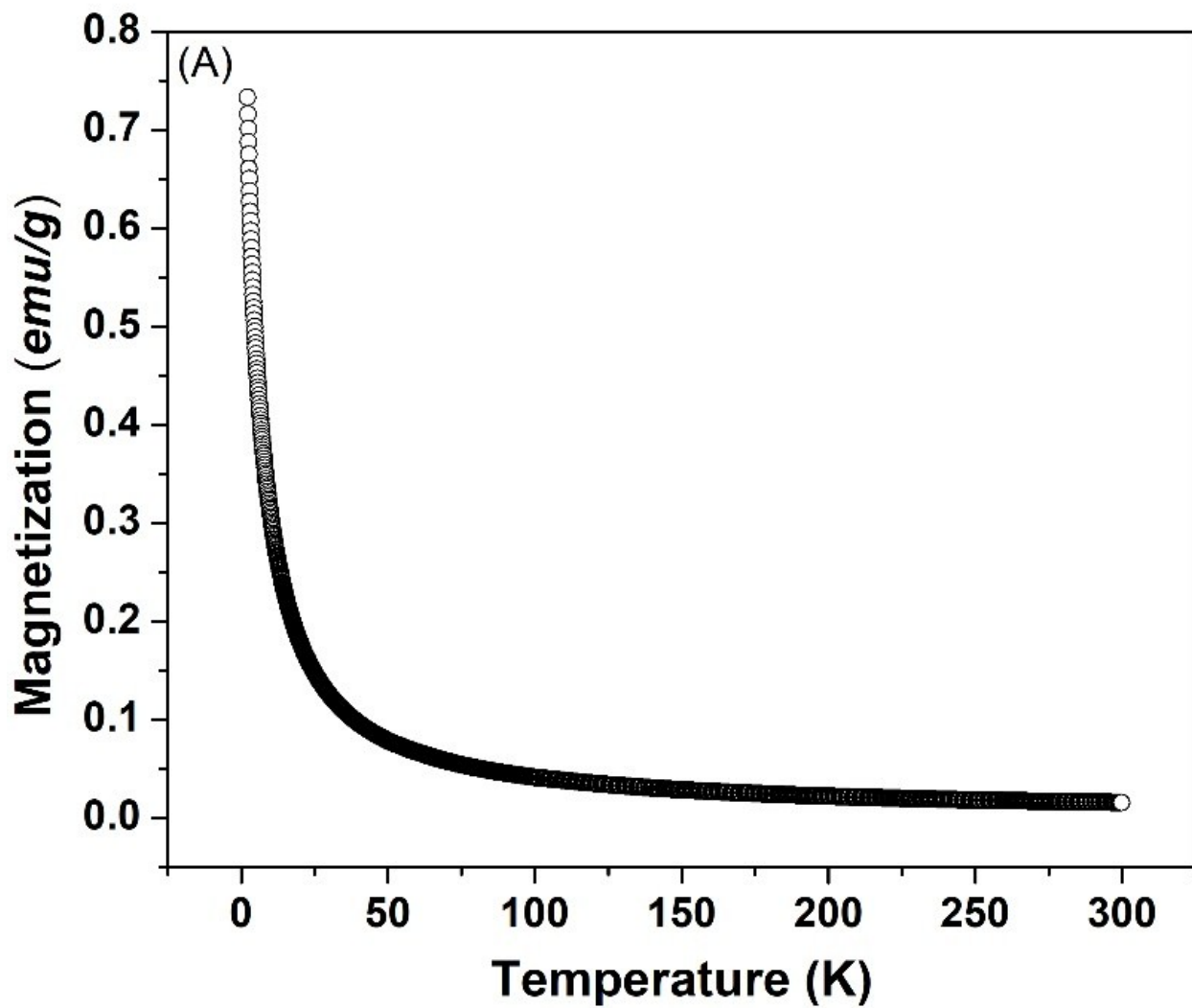


Fig. S11. Magnetization measurements of **1** for temperatures  $3\text{K} \leq T \leq 300\text{ K}$  with an applied field of 1000 Oe.

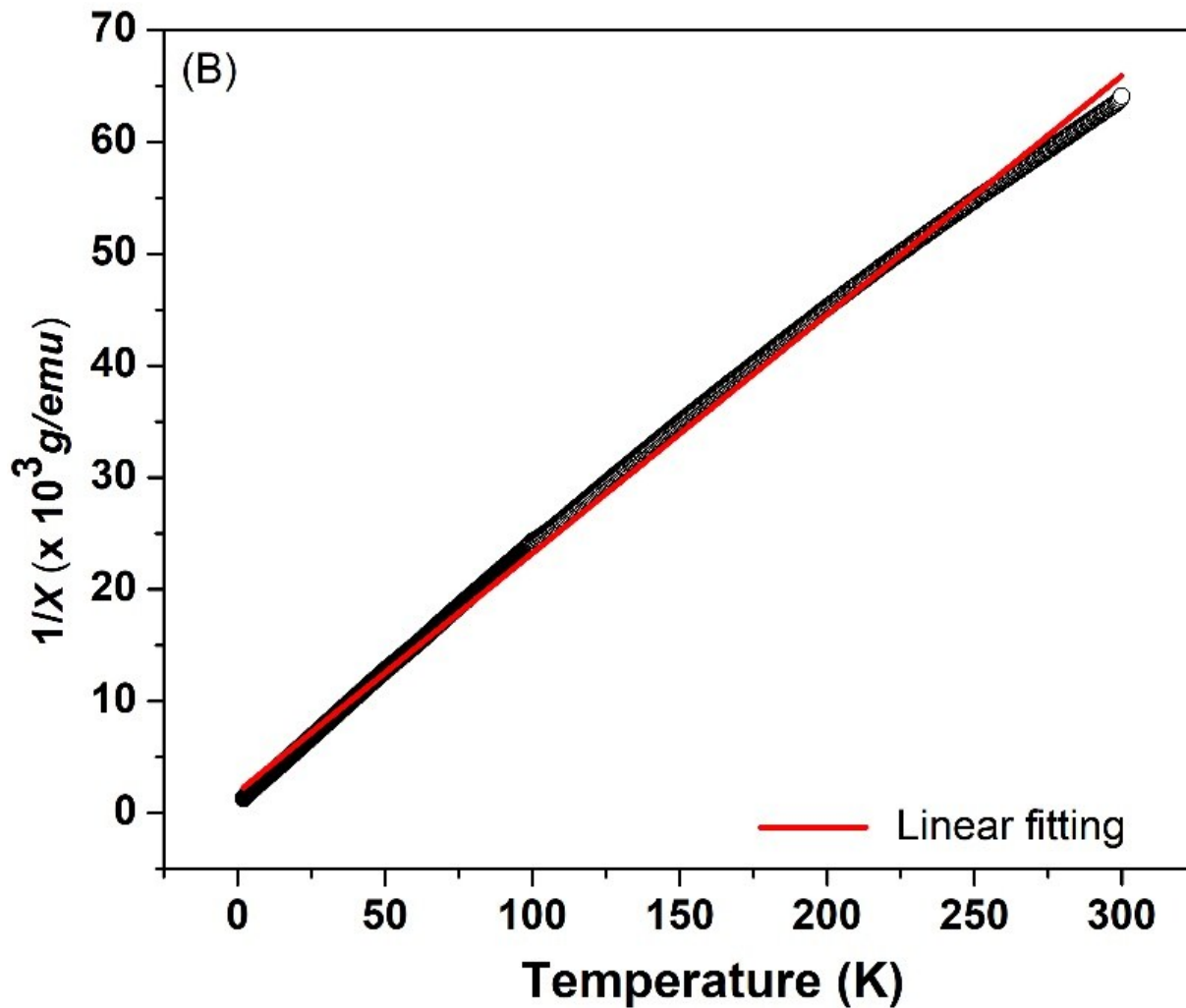


Fig. S12. Curie-Weiss fitting (red line) of the inverse mass susceptibility ( $1/\chi$ ) versus temperature of 1.

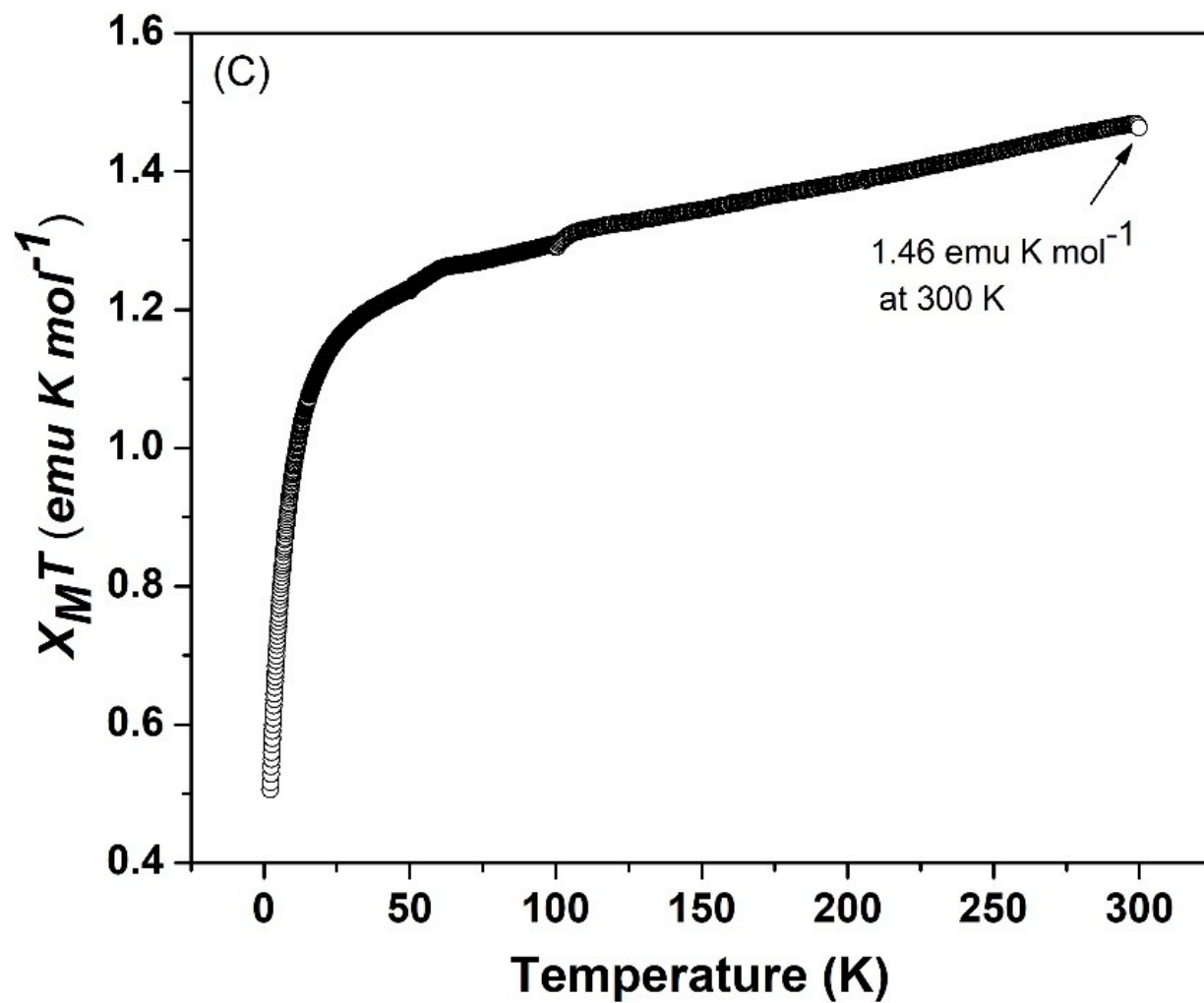


Fig. S13.  $\chi_M T$ -versus- $T$  plot of **1**

The corresponding temperature-dependent molar susceptibility per metal ion in **1** shows the  $\chi_M T$  value at 300 K of ca. 1.46 (emu K mol<sup>-1</sup>), suggesting the existence of Ni<sup>2+</sup> in **1**.<sup>6,7</sup>

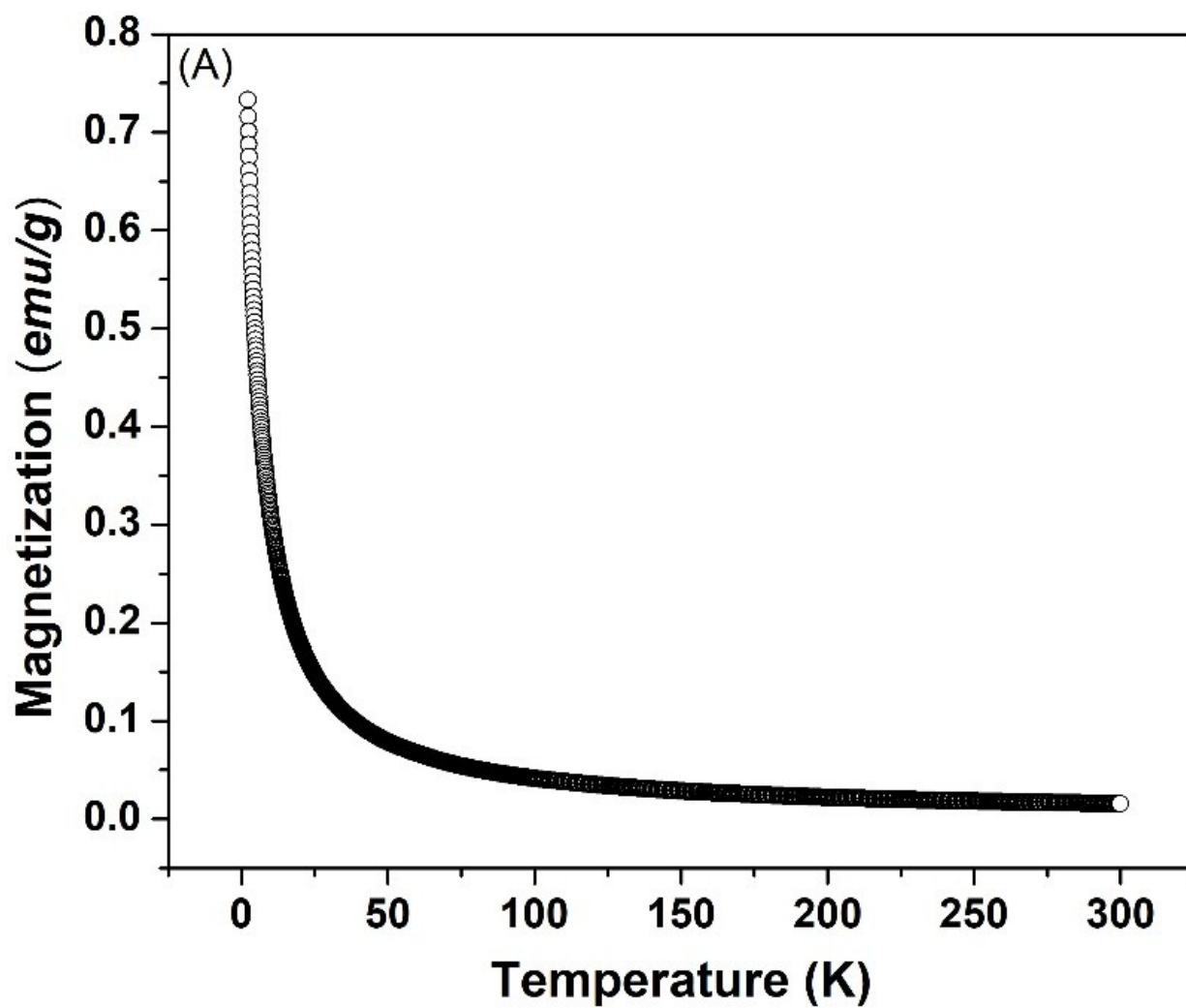
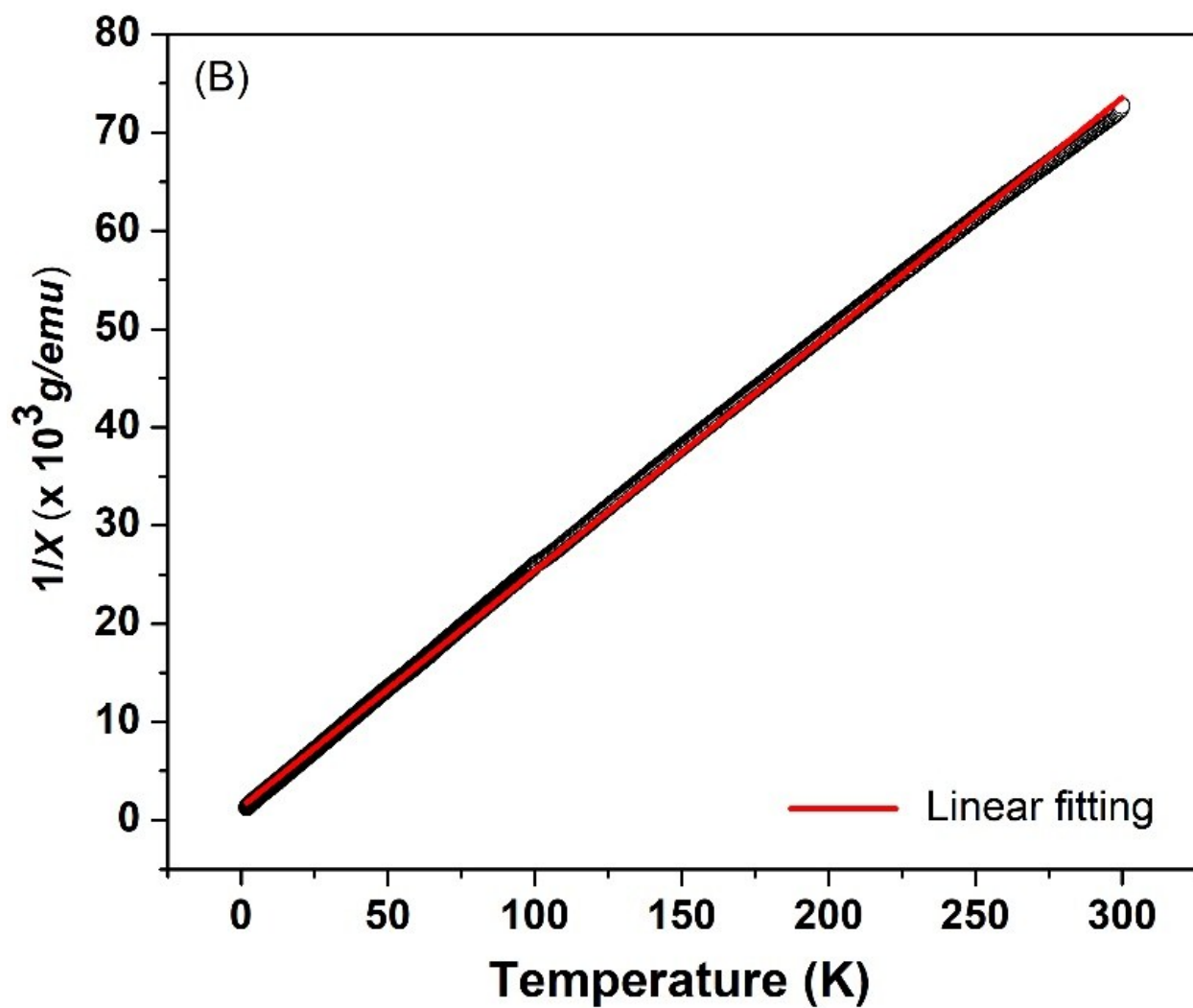


Fig. S14. Magnetization measurements of **2** for temperatures  $3\text{K} \leq T \leq 300\text{ K}$  with an applied field of 1000 Oe.



**Fig. S15.** Curie-Weiss fitting (red line) of the inverse mass susceptibility ( $1/\chi$ ) versus temperature of 2.

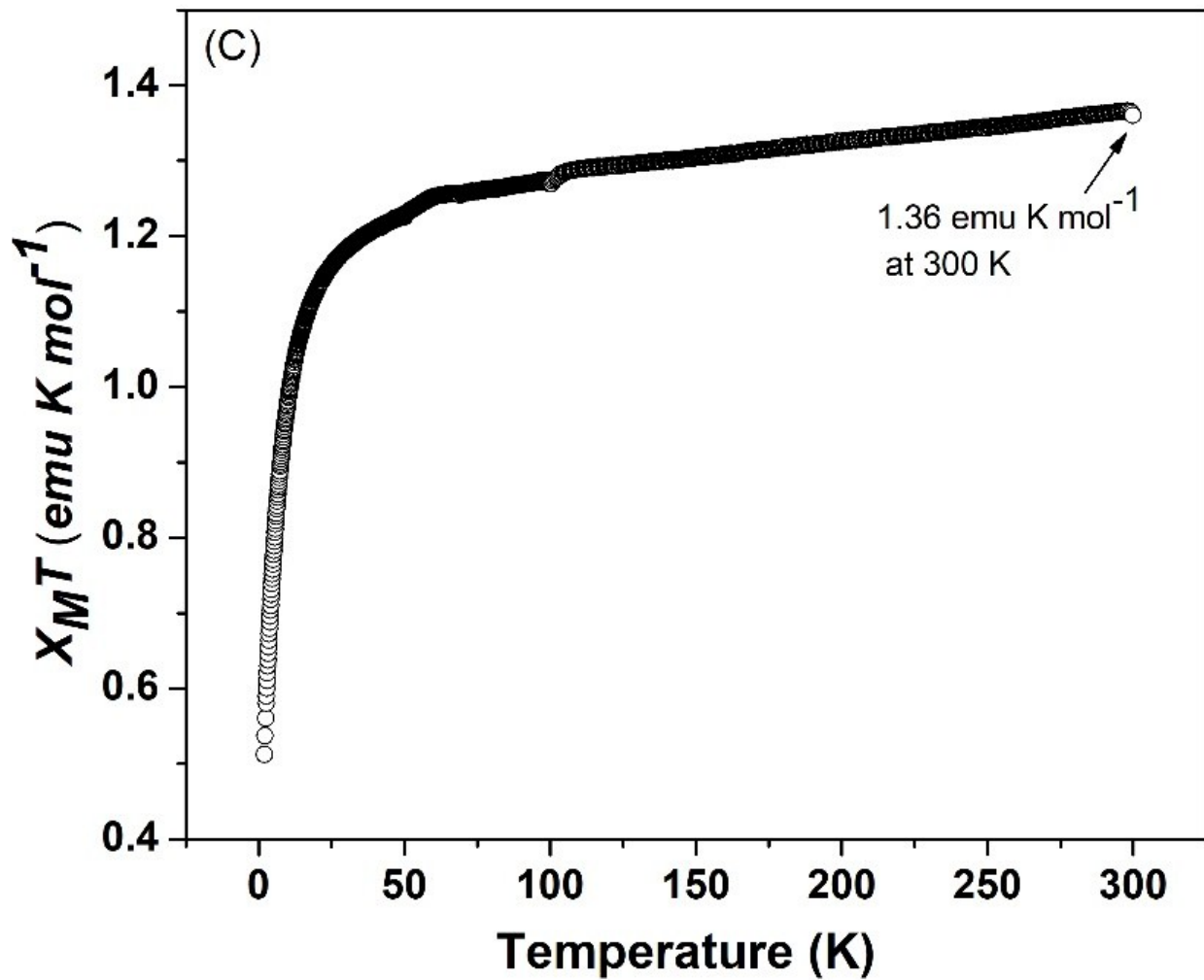
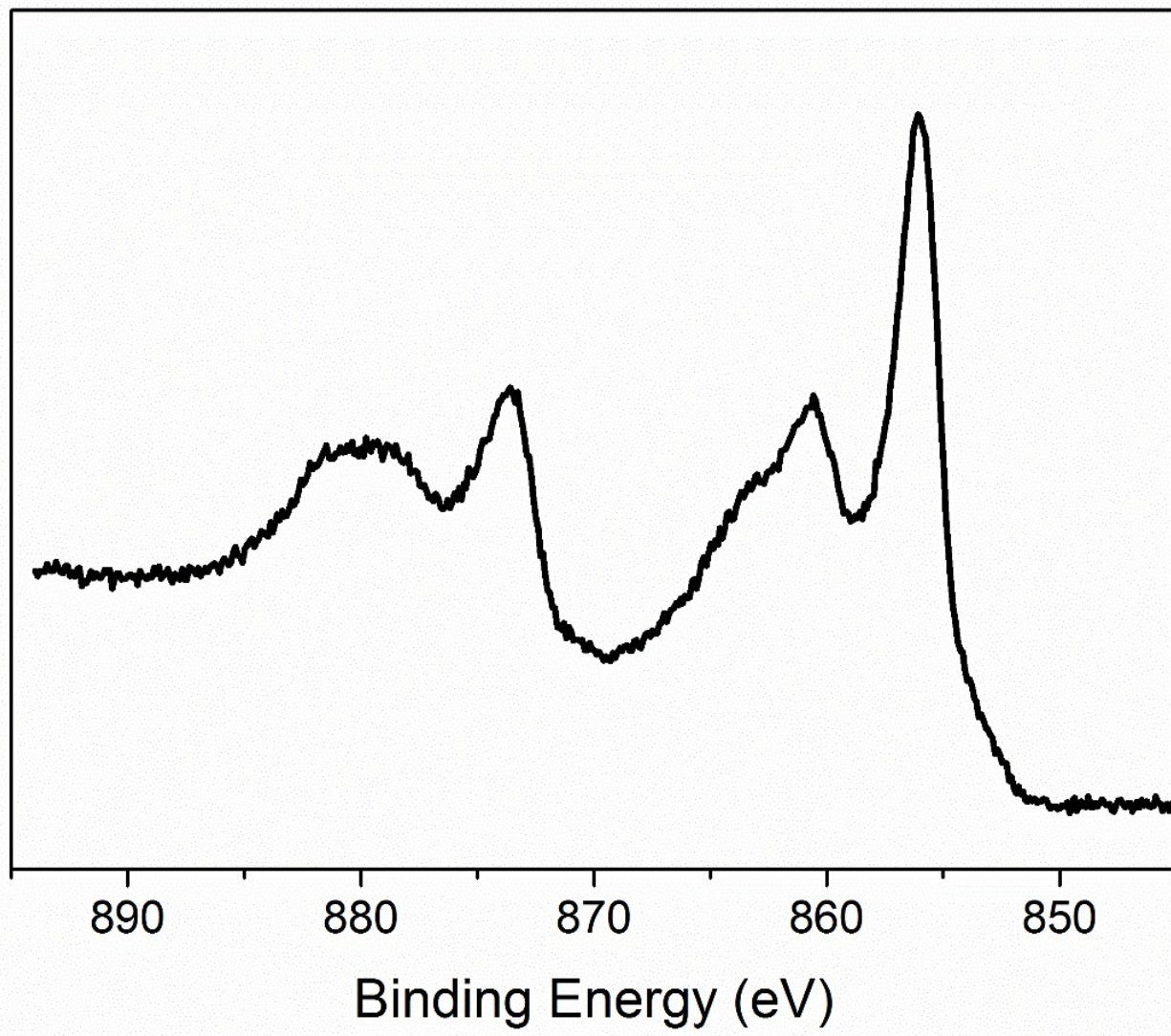


Fig. S16.  $\chi_M T$ -versus- $T$  plot of **2**

The corresponding temperature-dependent molar susceptibility per metal ion in **2** shows the  $\chi_M T$  value at 300 K of ca. 1.36 (emu K mol<sup>-1</sup>), suggesting the existence of Ni<sup>2+</sup> in **2**.<sup>6,7</sup>



**Fig. S17.** High-resolution XPS surveys for Ni 2p of **1**.

XPS for Ni 2p of **1** shows two intense peaks at 855.28 and 872.78 eV, which can be assigned to Ni 2p<sub>3/2</sub> and Ni 2p<sub>1/2</sub>, respectively. The data confirms the presence of Ni<sup>2+</sup> oxidation states in **1**.<sup>8</sup>

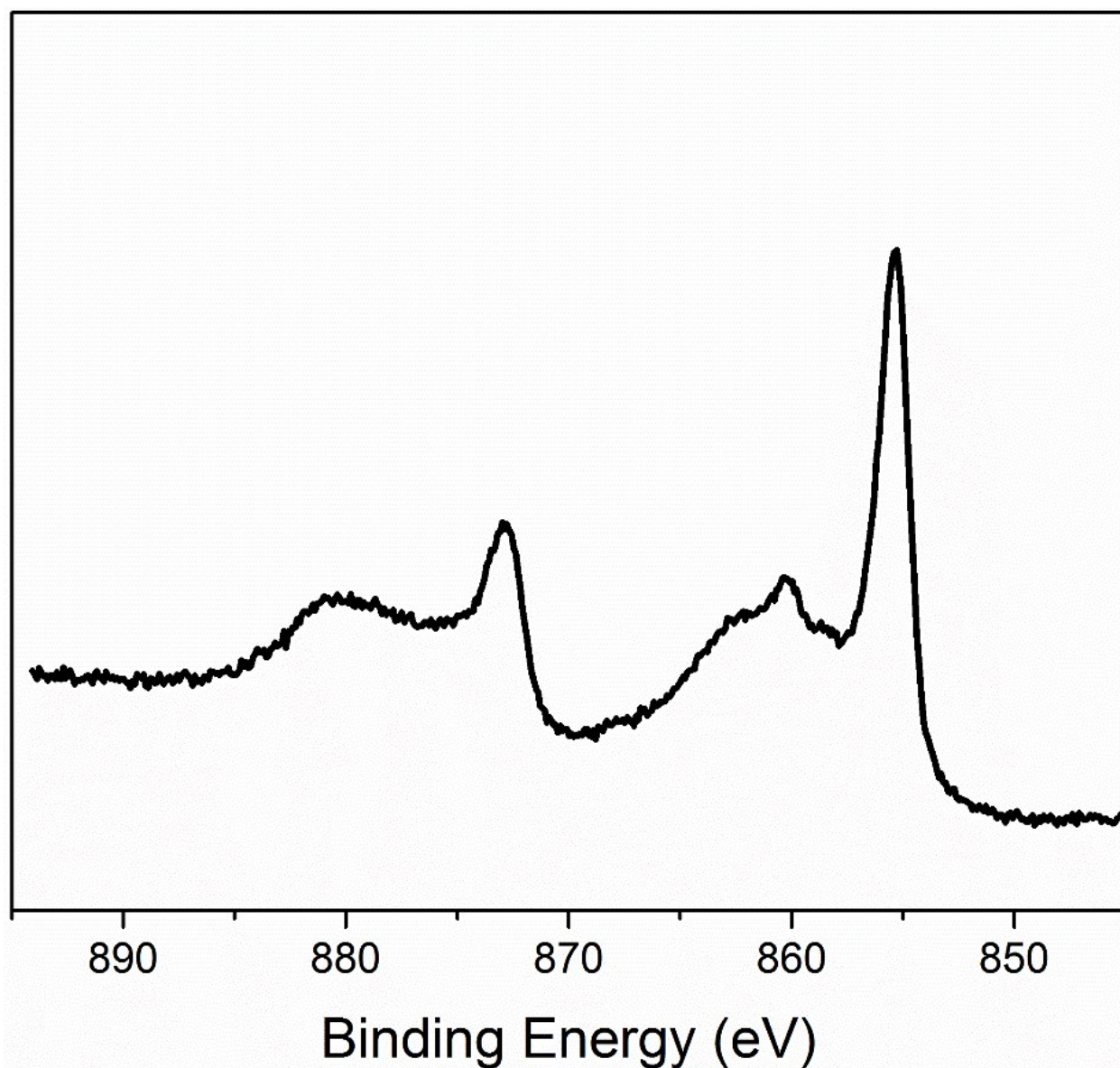


**Fig. S18.** High-resolution XPS surveys for Ni 2p of **2**.

XPS for Ni 2p of **2** shows two intense peaks at 856.03 and 873.88 eV, which can be assigned to Ni 2p<sub>3/2</sub> and Ni 2p<sub>1/2</sub>, respectively. The data confirms the presence of Ni<sup>2+</sup> oxidation states in **2**.<sup>8</sup>

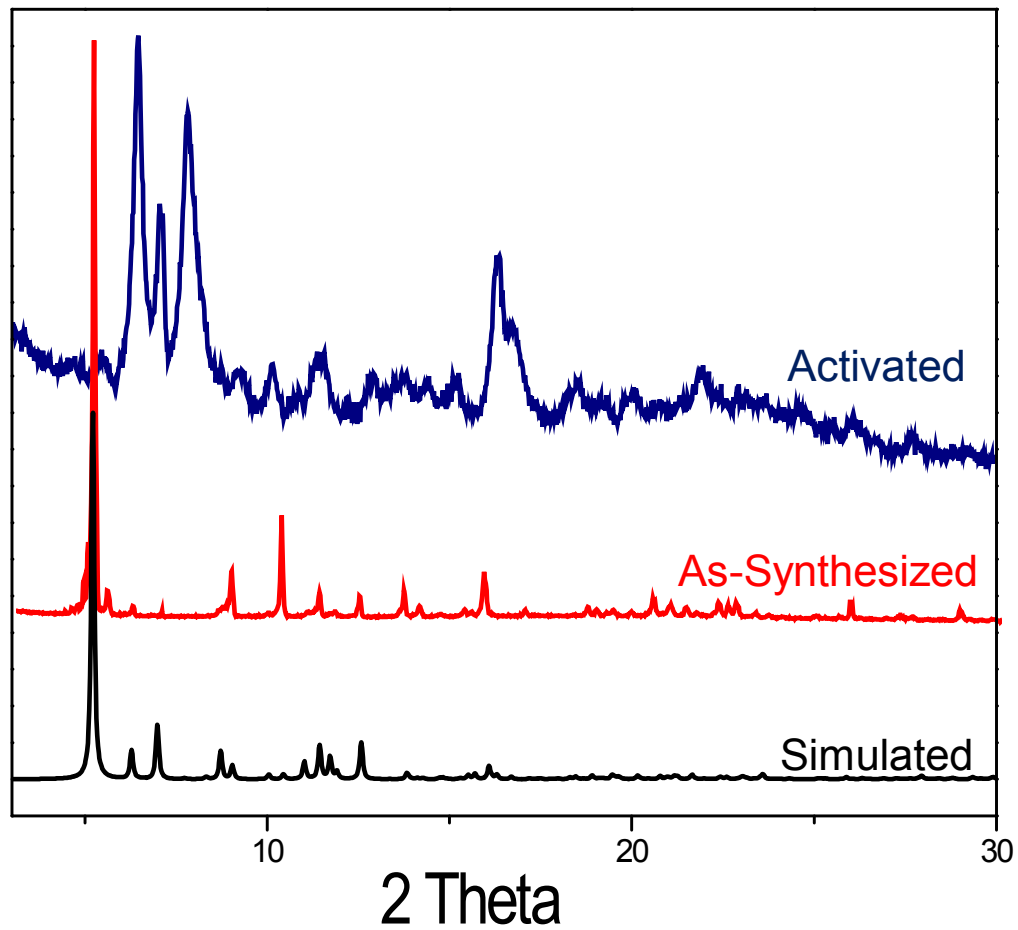


**Fig. S19.** Powder X-ray diffraction (PXRD) patterns for complex 1. Pattern simulated from single-crystal structure in black; experimental patterns for as-synthesized and activated (heating at 60 °C under a vacuum for 36 hours) in red and blue, respectively.

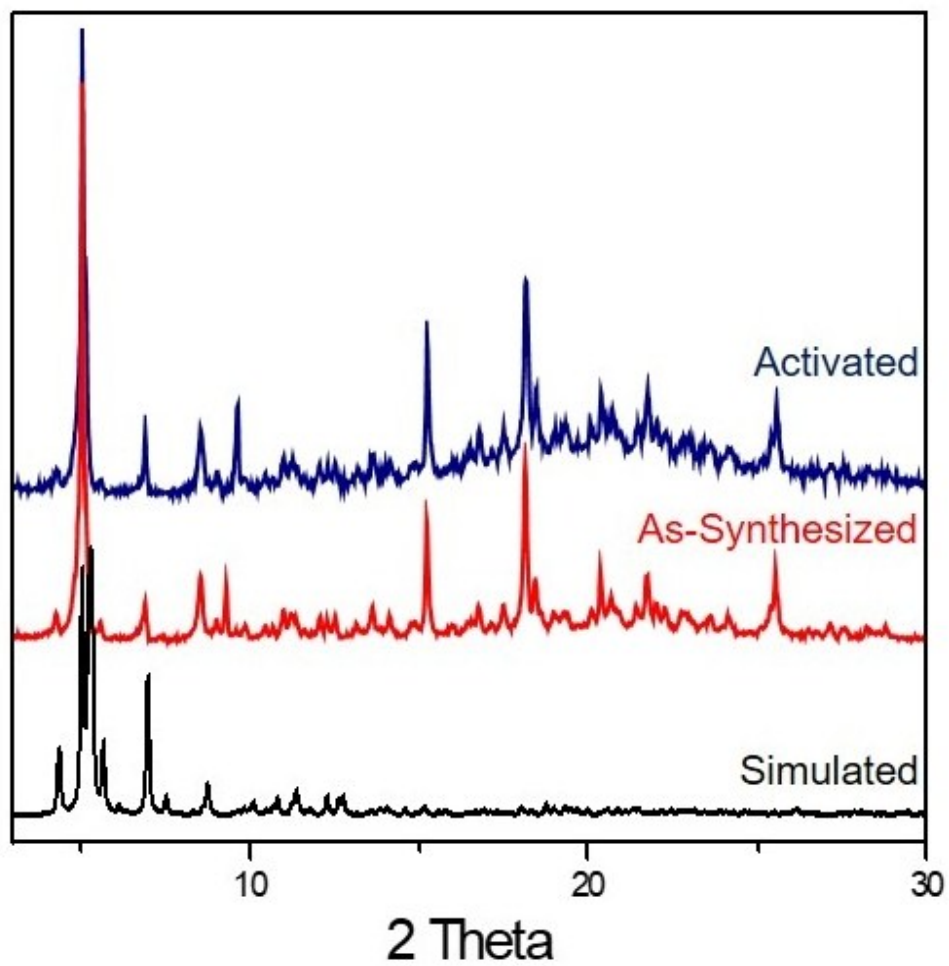


**Fig. S20.** Powder X-ray diffraction (PXRD) patterns for complex 2. Pattern simulated from single-crystal structure in black; experimental patterns for as-synthesized and activated (heating at 60 °C under a vacuum for 36 hours) in red and blue, respectively.

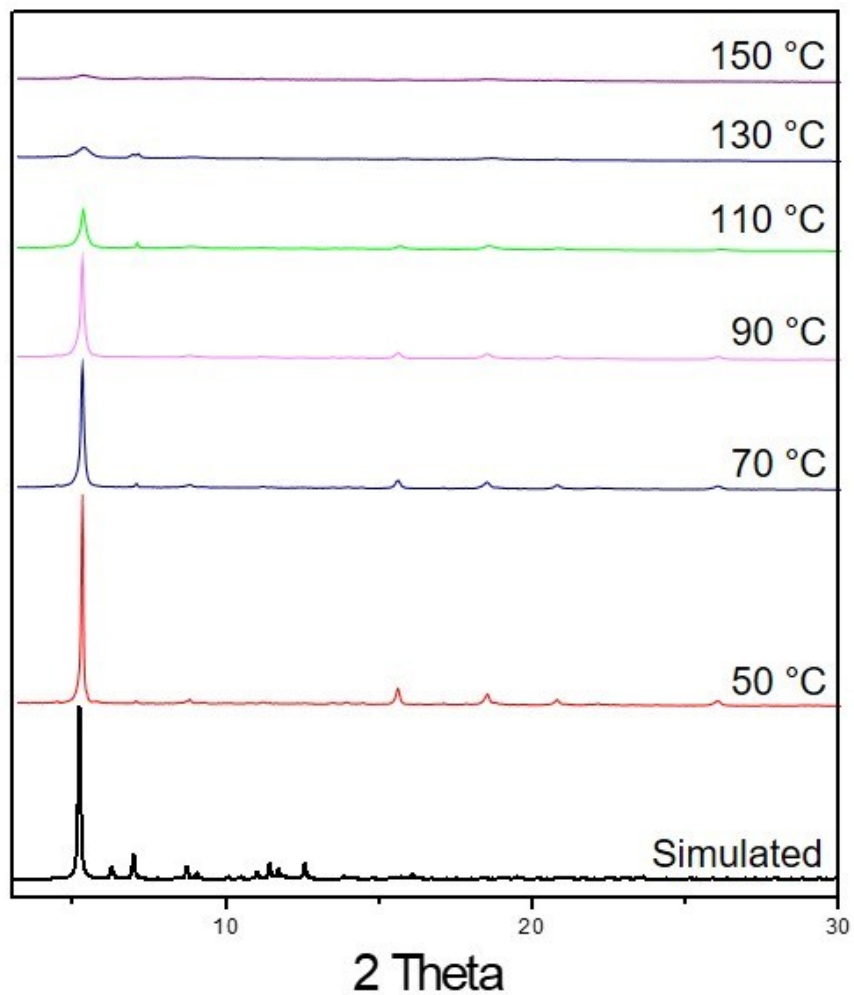


**Fig. S21.** PXRD patterns for complex **1** at different treating temperatures (50, 70, 90, 110, 130, and 150 °C). Pattern simulated from single-crystal structure in black.

- As-prepared samples were washed thoroughly with 5 mL of DMF (3 times) and 5 mL of acetone (3 times). The washed sample was mounted on the PXRD sample holder and the holder was heated at different temperature (50, 70, 90, 110, 120, 140, and 160 °C) for 30 min by using temperature-controlled.

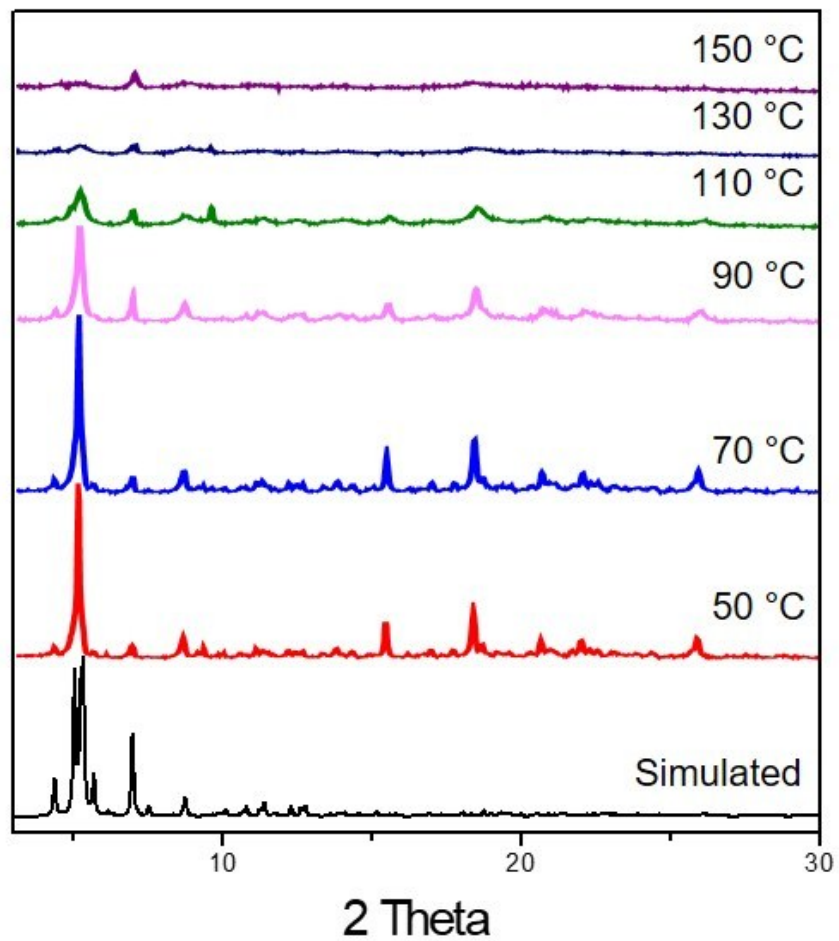


**Fig. S22.** PXRD patterns for complex **2** at different treating temperatures (50, 70, 90, 110, 130, and 150 °C). Pattern simulated from single-crystal structure in black.

- As-prepared samples were washed thoroughly with 5 mL of DMF (3 times) and 5 mL of acetone (3 times). The washed sample was mounted on the PXRD sample holder and the holder was heated at different temperature (50, 70, 90, 110, 120, 140, and 160 °C) for 30 min by using temperature-controlled.

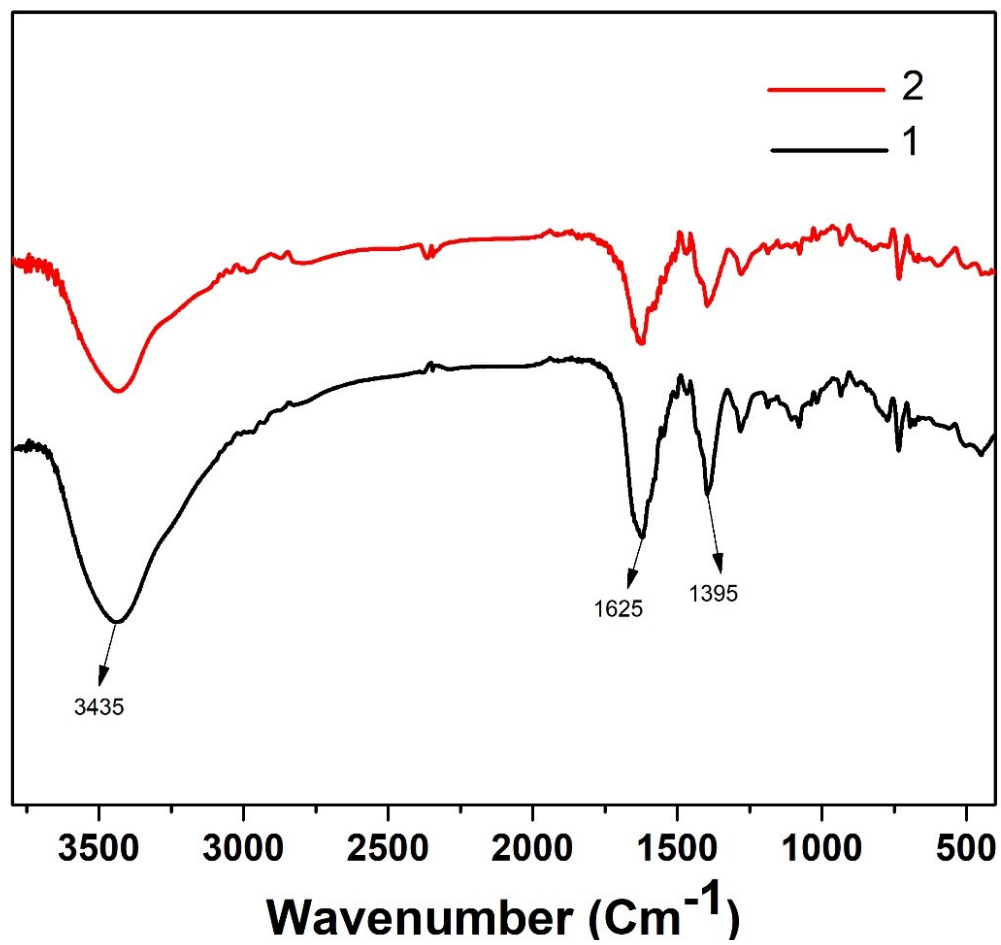
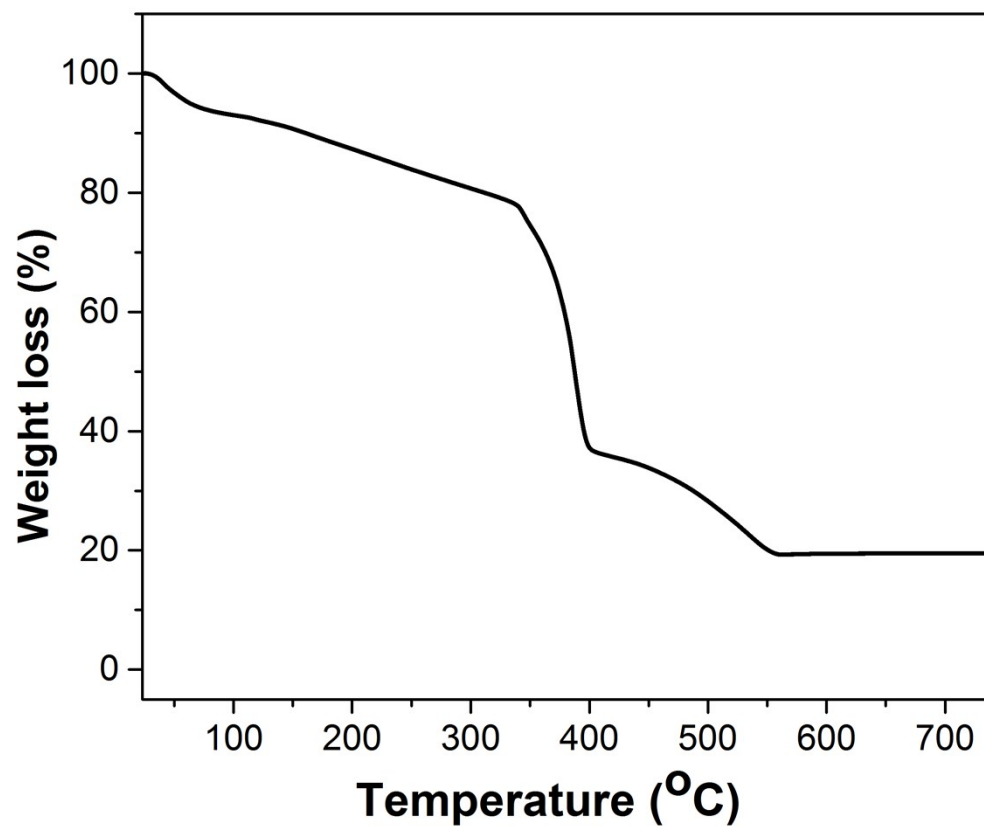
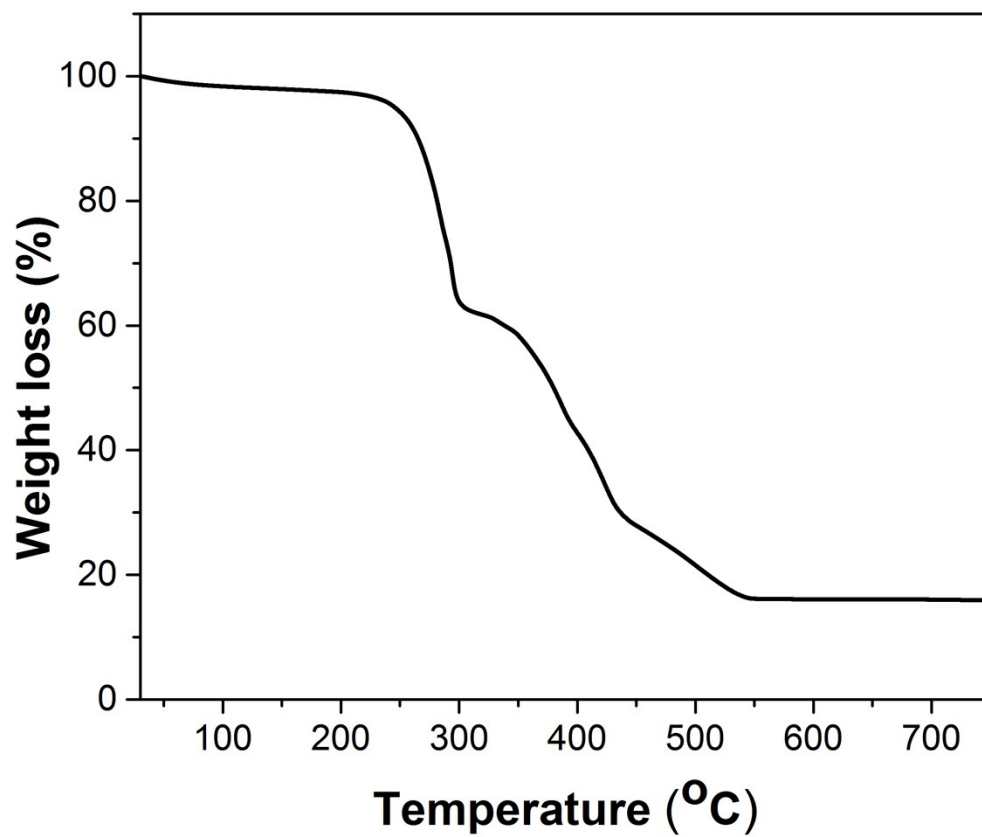


Fig. S23. IR spectra of 1 and 2.



**Fig. S24.** Thermogravimetric analysis (TGA) for **1**.



**Fig. S25.** Thermogravimetric analysis (TGA) for **2**.

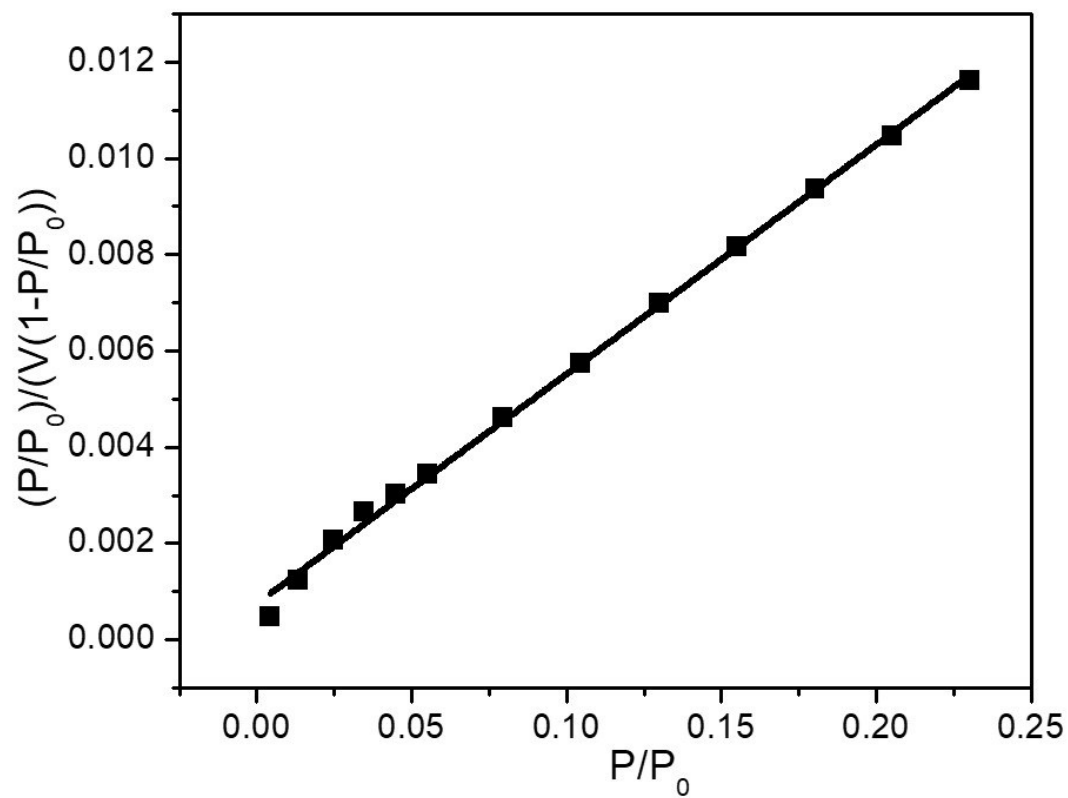


**Fig. S26.** Plot of  $(P/P_0)/(V(1-P/P_0))$  vs  $(P/P_0)$  derived from the corresponding  $\text{CO}_2$  adsorption at 196 K of **1**.

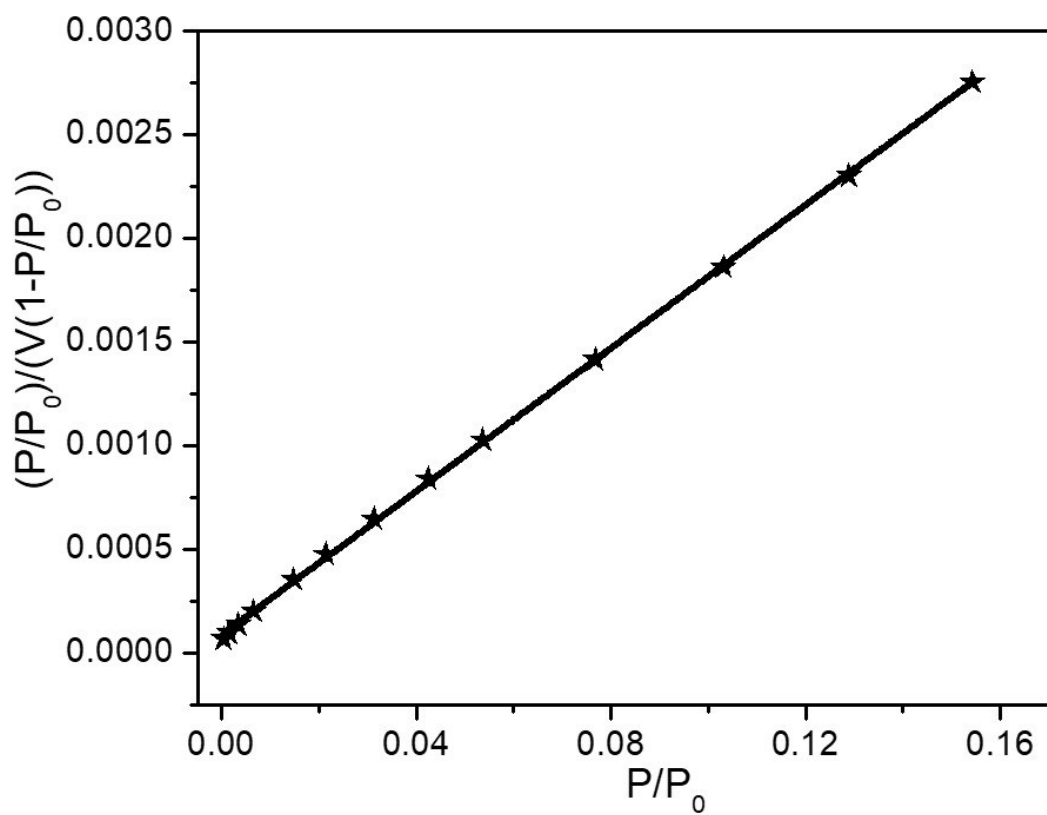


**Fig. S27.** Plot of  $(P/P_0)/(V(1-P/P_0))$  vs  $(P/P_0)$  derived from the corresponding  $\text{CO}_2$  adsorption at 196 K of 2.

## REFERENCES

1. A. J. Arvai and C. Nielsen, "ADSC Quantum-210 ADX Program" (Area Detector System Corporation: Poway, CA, USA, 1983).
2. Z. Otwinowski and W. Minor, Volume 276: Macromolecular Crystallography, part A, p.307-326, 1997, W. Carter, Jr. & R. M. Sweet, Eds., Academic Press (New York).
3. G. M. Sheldrick, *Acta Cryst. A*, 2015, **71**, 3-8.
4. G. M. Sheldrick, *Acta Cryst. C*, 2015, **71**, 3-8.
5. O. V. Dolomanov, L. J. Bourhis, R. J. Gildea, J. A. K. Howard and H. J. Puschmann, *Appl. Cryst.*, 2009, **42**, 339-341.
6. V. C. Thi Le, H. D. Mai, P. Kang and H. Yoo, *Chem. Eur. J.*, 2019, **25**, 2472-2476.
7. V. A. Neacșu, C. Maxim, A. M. Mădălan, M. Hillebrand, C. González-Arellano, S. Soriano, E. Rentschler and M. Andruh, *Polyhedron*, 2018, **150**, 77-82.
8. Y. Zhang, Y. Liu, M. Ma, X. Ren, Z. Liu, G. Du, A. M. Asiri and X. Sun, *Chem. Commun.*, 2017, **53**, 11048-11051.